Korean J. Chem. Eng., 37(3), 456-465 (2020)
DOI: 10.1007/s11814-019-0470-0

pISSN: 0256-1115
eISSN: 1975-7220

Interactive effect of pH and cation valence in background electrolyte solutions on simazine sorption to *Miscanthus* biochar produced at two different pyrolysis temperatures

Seoyeon Lee, Junho Han, and Hee-Myong Ro†

Department of Agricultural Biotechnology and Research Institute of Agriculture and Life Sciences, Seoul National University, Seoul 08826, Korea
(*Received 9 September 2019 • accepted 21 December 2019*)

Abstract−Biochar has considerable sorption efficiency for organic pollutants; however, the effect of physicochemical characteristics and their alteration by environmental conditions on the sorption mechanism is still unknown. We investigated the pH-dependent sorption of simazine on *Miscanthus* biochar produced at two pyrolysis temperatures (400 and 700 °C; hereafter B-400 and B-700) under two different electrolytes and interpreted the sorption mechanism. The surface charge density (SCD) decreased more in B-400 than in B-700 at higher pH due to more deprotonation of acidic functional groups (AFGs), but greater decreases were observed in B-700 than in B-400 from pH 2 to pH 3 as a result of alkali salts deposition. The decrease in K_F with increasing pH showed that simazine sorption decreased as van der Waals forces because the surface of biochar carried a greater negative SCD, which repulses simazine molecules due to the enhanced deprotonation of AFGs. At a given pH, K_F was lower in $CaCl_2$ than in NaCl due to the formation of larger metal-biochar complexes, resulting in enhanced blocking of pores available for simazine sorption. We believe that knowledge of the pH-dependence of SCD and accessibility of biochar pores could help better interpret the behavior of simazine-like pollutants in soil and aquatic environments.

Keywords: Simazine, Electrolyte, Biochar, Sorption, Isotherm, pH, Cation Valence

INTRODUCTION

Biochar is a carbonaceous material produced through pyrolysis of various forms of agricultural biomass under oxygen-limited conditions [1,2], resulting in diverse physicochemical characteristics (PCs). Agricultural biomass and pyrolysis temperature (PT) are key factors that determine the PCs of biochar [3,4], since thermal decomposition of specific molecular structures in agricultural biomass requires specific PTs [5,6]. As cellulose degrades at 220-315 °C, hemicellulose degrades at 315-400 °C and lignin degrades at >400 °C [5,6] during pyrolysis, increased PT causes an increase in aromatic C structures on the surface of plant-derived biochar [7] due to progressive polymerization [8]. As a result, biochar produced by pyrolysis at different PTs will have different specific surface area (SSA) and surface hydrophilicity/hydrophobicity properties; thus, biochar can serve as a cost-effective [9,10], environmentally sound solution in the effective remediation of organic pollutants under various environmental conditions [11,12]. However, the efficiency of remediation using biochar has not been fully investigated, or understood, in terms of the interactions of organic pollutants with various types of biochar due to insufficient knowledge of the PCs of biochar; thus, adverse effects or unprecedented results have frequently been reported in recent investigations [13-15]. Therefore, understanding the sorption mechanisms of biochar for organic pollutants in relation to the PCs of biochar is a prerequisite for interpreting the interactions between organic pollutants and biochar in real environments.

Under various environmental conditions, the relationship between the PCs of biochar and sorption mechanisms may vary, depending mainly on pH and background electrolyte, and this difference in turn affects the interactions of organic pollutants with biochar [16,17]. Acidic functional groups (AFGs) on the surface of biochar are mainly responsible for the remediation of organic pollutants [18,19], and their concentrations can be measured by Boehm titration, which quantifies carboxylic, lactonic and phenolic acidic groups [20]. Since each oxygen-containing AFG has a negative logarithmic acid dissociation constant (pK_a), when the pH is higher than the pK_a, it is negatively charged due to deprotonation [21,22]. Moreover, the surface charge density (SCD) of biochar becomes more negative with increasing pH, since further increases in pH deprotonate carboxylic ($pK_a \backsimeq 4.4$), lactonic ($pK_a \backsimeq 8.2$) and phenolic ($pK_a \backsimeq 10$) acidic groups [23]. When the pH is lower than the point of zero net charge (PZNC), the surface of biochar is positively charged, and the degree of protonation decreases with increasing pH; otherwise, the surface is negatively charged [24,25]. As a consequence, charged biochar can repel neutral organic pollutants but attract charged organic pollutants [26,27]. Concurrently, charged biochar can interact with background electrolytes, which affect the ionic atmosphere of the solution, to achieve electrostatic stabilization [28]. Therefore, understanding the behavior of simazine and biochar across an environmental pH range with varying background electrolytes is necessary to study the mechanism of simazine sorption to the surface of biochar. However, despite current knowledge

†To whom correspondence should be addressed.
E-mail: hmro@snu.ac.kr

regarding the effect of pH and background electrolytes on the sorption mechanism, the interactions of simazine molecules on the surface of biochar remain largely unknown due to the heterogeneity of biochar [17].

Simazine [2-chloro-4,6-bis(ethylamino)-s-triazine] is a herbicide that has lone-pair electrons in its nitrogen-containing heterocyclic structure that inhibits the photosynthetic electron transport process in annual grasses and broadleaf weeds [29]. Due to its remarkably efficient weed control, simazine has been widely used as a nonselective herbicide since its introduction in 1956 [30]. However, recent evidence has shown that simazine poses threats to the environment and to human health because of its persistence and accumulation, resulting from its low solubility and non-volatility [30]; triazines can cause hormonal disruption and damage to the kidneys and thyroid [31,32]. Therefore, the removal or remediation of simazine from polluted soils is urgent; nevertheless, the pH-dependence of the sorption mechanism of simazine to biochar needs to be better understood to properly assess the risks and threats from the environmental problems associated with simazine under natural environmental conditions. At pH values below its pK_a of 1.7 [30], simazine, which is an organic base, is positively charged due to protonation, while it is neutral above this pK_a [33]; thus, the sorption mechanisms of simazine to biochar are pH-dependent. Therefore, knowledge of the behavior of simazine and biochar across at least the surrounding environmental pH and background electrolyte conditions is essential to interpret the sorption mechanisms of simazine to biochar and develop suitable remediation technology for real environments.

We hypothesized that changes in PT alter the surface morphology and charge characteristics of biochar and that the PT-driven sorption behavior of biochar varies with pH, cation valence (CV) and their interaction in background electrolyte solution, thus changing the sorption capacity and mechanism of simazine sorption to biochar. Here, we tested this hypothesis by interpreting the effects of pH, CV and their interactions on PT-driven simazine sorption. We conducted batch sorption isotherms of simazine to *Miscanthus* biochar produced at two different PTs (400 and 700 °C) under different pH and CV conditions in background electrolyte solutions, fitted the experimental sorption data to sorption isotherm models, measured the SCD and morphological characteristics of biochar before and after treatment, and analyzed the effect of pH, CV and their interaction on simazine sorption to biochar.

MATERIALS AND METHODS

1. PCs of Biochar

Biochar was produced from *Miscanthus* feedstock at different PTs (400 and 700 °C) (hereafter, B-400 and B-700, respectively) to distinguish the PCs based on thermal decomposition, which occurred below or above a PT of 500 °C [34-36]. The rate of heating was approximately 10 °C min^{-1}, and the target temperatures were maintained for 1 h for the completion of pyrolysis under N_2 gas purging. Biochar was ball-milled (MM400, Retsch, Germany) and sieved through a 106-μm mesh to minimize the size effects [17]. The SSA was determined using the Brunauer-Emmett-Teller (BET) isotherm with N_2 and CO_2 gas adsorbates because N_2 (ASAP 2010, Micromeritics, USA) is sorbed only on micro-pores (>1.5 nm), while CO_2 (BELSORP-mini II, Microtrac BEL, Japan) is sorbed on both micro- and nano-pores (<1.5 nm) [37]. Biochar particles were separated into three fractions (<25, 25-53 and 53-106 mm) using Analysette 3 pro (Fritsch, Germany). The mass percent of carbon (C), hydrogen (H), nitrogen (N) and sulfur (S) was analyzed using an elemental analyzer (Flash 2000, Thermo, USA), and that of O (oxygen) was calculated by subtracting %C, %H, %N and %S from 100%.

The AFGs were determined by Boehm titration [38,39]. Since the results of Boehm titration can be affected by dissolved salts, biochar was pretreated with dilute HCl at pH 2 for three days followed by washing with deionized water until the $AgNO_3$ test for Cl^- ions was negative and then oven dried at 80 °C for 24 h [40]. After pretreatment, biochar (0.2 g) was added to 20 mL of 0.05 M of three base solutions ($NaHCO_3$, Na_2CO_3 and NaOH) for 24 h and shaken on a flask shaker at 160 rpm (DS-300L, Dasol, Korea). Then, biochar suspension was separated by centrifugation (MF-600 plus, Hanil, Korea) for 40 min at 4,000 rpm. Ten milliliters of the supernatant was back-titrated with 0.01 M HCl using an automatic titrator (702 SM Titrino, Metrohm, Switzerland). The AFGs were estimated on the assumption that 0.05 M $NaHCO_3$ neutralizes carboxyl groups, 0.05 M Na_2CO_3 neutralizes carboxyl and lactonic groups, and 0.05 M NaOH neutralizes carboxyl, lactonic and phenolic groups.

Ash content of biochar was estimated by the combustion method, in which the residual weight was measured after heating at 750 °C for 6 h [41]. The electrical conductivity (EC) and pH were measured in a 1 : 20 (w/v) biochar/water suspension with an EC meter (Orion 3 star, Thermo, USA) and a pH meter (Orion 3 star, Thermo, USA) after shaking for 1.5 h [42]. The PZNC was determined using the pH drift method [43]. Approximately 60 mg of biochar was mixed with 20 mL of 0.05 M $CaCl_2$, and the pH was adjusted using 0.5 M HCl or 0.5 M NaOH. Then, the sample was shaken for 24 h on a flask shaker at 160 rpm. The pH was measured with a pH meter and plotted against the initial pH, with the PZNC taken at the equal point between the initial and final pH. The concentration of inorganic elements was analyzed using X-ray fluorescence (XRF) (S4 Pioneer, Bruker, USA).

2. SCD and Morphological Characteristics of Biochar

All reagents were purchased from Sigma-Aldrich (St. Louis, MO, USA). The SCD of biochar was measured by the potentiometric titration method [44]. To achieve complete protonation of AFGs, biochar (1 g) was added to 100 mL of 0.05 M $CaCl_2$ solution in a 250 mL Duran laboratory glass bottle sealed with a PTFE cap, and the mixture was equilibrated by shaking on a vial shaker (DS-300L, Dasol, Korea) at 160 rpm for three days at 25±0.5 °C. During equilibration, the suspension was adjusted daily to pH 2 using 1 M HCl solution, and then 0.01 M NaOH solution (titrant) was added dropwise to the acidic suspension (pH 2) using an automatic titrator to raise the pH to 11. The volume of titrant consumed and the corresponding pH were recorded in 10 s intervals during the titration. A blank titration was repeated without biochar to correct for the volume of titrant consumed. The SCD, $\delta_{0,H}$ (C m^{-2}), was calculated from the points on the titration curve as follows:

$$\Gamma_{H^+} + \Gamma_{OH^-} = \frac{C_{NaOH}(V_b - V_a)}{s \cdot \gamma \cdot V} \quad (1)$$

$$\delta_{0,H} = F(\Gamma_{H^+} + \Gamma_{OH^-}) \quad (2)$$

where Γ_{H^+} and Γ_{OH^-} (mol m^{-2}) are the concentrations of H^+ and OH^- on the surface of biochar, respectively, C_{NaOH} (mol L^{-1}) is the concentration of titrant, V_b and V_a (L) are the volumes of titrant added in the blank and analyte (biochar) titrations, respectively, s (m^2 kg^{-1}) is the SSA, γ (kg L^{-1}) is the mass concentration, V (L) is the total volume of the solution, and F (C mol^{-1}) is the Faraday constant.

The morphology and elemental composition of biochar after simazine sorption at different pH values and CVs in background electrolyte solutions were analyzed with a field emission-scanning electron microscope (FE-SEM) (AURIGA, Carl Zeiss, Germany) equipped with an energy dispersive X-ray spectroscopy (EDS) detector (Bruker Nano GmbH, Berlin, Germany). For FE-SEM analysis, biochar samples were placed in a forced-air oven (DS-80-2, Dasol, Korea) at 80 °C for at least 48 h and then mounted on an aluminum stub using double-sided conductive copper tape. The microscope was operated at an accelerating voltage of 10 kV, and the working distance was set at 10 nm from the final lens at varying magnifications.

3. Sorption Isotherm Experiment

All reagents were purchased from Sigma-Aldrich (St. Louis, MO, USA), and an aqueous standard solution of simazine was prepared by diluting the simazine stock solution in methanol (99.8% purity) [17]. Five milliliters of the simazine stock solution (20 mg L^{-1}) was mixed with 10 mL of 0.2 M NaCl or 0.1 M $CaCl_2$ solution and biochar (0.2 g) in a 30 mL amber glass vial with a Teflon-lined cap to prevent photodegradation of simazine [30]. The pH was adjusted to 3.5, 7.5 and 10 using 1 M HCl or 1 M NaOH, and distilled water was added to make a total volume of 20 mL; the final solution contained simazine (5 mg L^{-1}, the maximum solubility), NaCl (0.1 M) and $CaCl_2$ (0.05 M). Each sample was equilibrated by shaking on a flask shaker at 160 rpm for 81 h at 25± 0.5 °C, and the pH was readjusted daily during equilibration. Each mixture was filtered through a 0.45-μm nylon membrane filter to separate simazine from biochar matrix. For the determination of simazine concentrations, 10 mL of each filtrate was shaken vigorously after adding 2 mL of hexane, and one milliliter of supernatant was transferred to a 2 mL amber vial with a rubber cap for GC analysis. To ensure the quality of the data collection (accuracy and precision), all batch sorption experiments were performed in triplicate according to the US Environmental Pretention Agency (US EPA) [45].

The simazine concentration was measured using a gas chromatograph with micro-electron capture detector (GC-μECD) (6890N, Agilent Technologies Inc., USA) with a silica capillary column (HP-5, 0.32 mm i.d.×30 m×0.25 μm) [46]. The inlet and detector temperatures were 250 °C and 300 °C, respectively, and the carrier gas was N_2 with a flow rate of 1.2 mL min^{-1} under constant flow mode. The oven temperature was set as follows: initial temperature of 50 °C (held for 1 min), 20 °C min^{-1} to 150 °C (held for 4 min), 3 °C min^{-1} to 230 °C (held for 1 min), and finally 10 °C min^{-1} to 300 °C (held for 5 min). The total analysis time per sample was 50 min and the retention time for simazine was 19 min. All calibrations were performed in ChemStation (Agilent, USA). To guarantee the stability of GC-μECD measurements, the instrument calibration was performed by analyzing the standard simazine solutions and plotting the relative response factors of analyte in each batch sorption experiment.

4. Data Calculation and Fitting

The concentration of simazine sorbed on biochar (q_{eq}, mg kg^{-1}) was calculated from the difference between the initial and equilibrium concentrations of simazine in solution (Eq. (3)):

$$q_{eq} = \frac{(C_0 - C_{eq}) \times V}{m} \quad (3)$$

where C_0 and C_{eq} are the initial and equilibrium concentrations of simazine (mg L^{-1}) in solution, respectively, V is the volume of solution (L), and m is the mass of biochar (kg).

The sorption isotherm results constructed at pH 3.5, 7.5 and 10 were fitted to the Langmuir and Freundlich isotherm models to simulate the sorption process of simazine to biochar [39,47]. The Langmuir model, which describes ideal monolayer adsorption, is expressed as follows (Eq. (4)):

$$q_{eq} = \frac{q_{max} \cdot K_L \cdot C_{eq}}{(1 + K_L \cdot C_{eq})} \quad (4)$$

where q_{max} is the maximum sorption capacity (mg kg^{-1}) and K_L is a constant related to energy (L mg^{-1}). The linear form of the Freundlich model, which describes nonideal sorption in multilayers and is based on heterogeneous surfaces with non-uniform distribution energy, is expressed as follows (Eq. (5)):

$$\log q_{eq} = \log K_F + \frac{1}{n} \log C_{eq} \quad (5)$$

where K_F is the equilibrium constant indicating sorption capacity (mg kg^{-1} (mg $L^{-1})^{-n}$) and 1/n is the sorption intensity.

To assess the applicability of the sorption isotherm model, the percent normalized standard deviation (Δq) was calculated as follows [48,49] (Eq. (6)):

$$\Delta q = 100 \sqrt{\frac{\sum_{i=1}^{n} \left[\left(\frac{q_{exp} - q_{cal}}{q_{exp}} \right)_i \right]^2}{n - 1}} \quad (6)$$

where q_{exp} and q_{cal} are the measured and estimated amounts of simazine sorbed on biochar for each data point (mg kg^{-1}), respectively, and n is the number of experimental measurement data points.

5. Statistical Analysis

Data were analyzed using the general linear model (GLM) procedure in SPSS software (SPSS Inc., Version 25.0, Chicago, IL, USA). The effects of two factors (pH and CV) and their interaction on the fitting parameters for the Freundlich and Langmuir isotherms were evaluated for each biochar, B-400 and B-700. Two-way analysis of variance (ANOVA) of a completely randomized design with three replications per treatment was performed to test for significant differences among the treatment means within each factor and for interactions between factors. The least significance difference (LSD) test at the significance level of $p<0.05$ was used to separate means.

RESULTS AND DISCUSSION

1. PCs of Biochar

The SSA was estimated at 5.6 $m^2 g^{-1}$ for micro-pores and 191.6 $m^2 g^{-1}$ for nano-pores in B-400, and 236.3 $m^2 g^{-1}$ and 57.2 $m^2 g^{-1}$, respectively, in B-700 (Table S1). Previous investigations on *Miscanthus* biochar reported that SSA of biochar increased with increasing PT [11,50]. The SSA of micro-pores of this biochar sharply increased from 10.97 to 443.92 $m^2 g^{-1}$ by increasing PT from 300 °C to 700 °C, while that of nano-pores gradually decreased from 110.83 to 11.04 $m^2 g^{-1}$ [51]. An increase in SSA of micro-pores with a concurrent decrease in SSA of nano-pores with increasing PT can be explained by progressive volatilization of specific molecular structures such as cellulose, hemicellulose and lignin, leading to formation of channel structures of larger pore-size and thereby increasing the quantity of micro-pores [6,52]. The percentage of particles having a given equivalent diameter (<25 μm, 25-53 μm and 53-106 μm) was 14.7, 52.8 and 32.5% for B-400, and 5.6, 62.0 and 22.4% for B-700, respectively.

Some atomic ratios could be used to characterize the aromaticity, hydrophobicity and polarity of biochar [17], and the ratio of (O+N)/C, O/C and H/C can be proxies of polarization, carbonization and hydrophilization of biochar, respectively [58,59]. In this study, the ratios of the corresponding values at higher PT (B-700) were lower than those at lower PT (B-400) (Table S1). In other words, the ratio of (O+N)/C, O/C and H/C of *Miscanthus* biochar decreased from 0.37 to 0.25, 0.36 to 0.24 and 0.05 to 0.01, respectively, as a result of increased C and decreased H, O, N and S content. With the decrease in the ratio of (O+N)/C, O/C and H/C, we inferred that polarity and the hydrophilicity of biochar decreased while aromaticity increased due to increased carbonization [18,53]. Previous investigations reported that *Miscanthus* biochar produced at 400 °C had the atomic ratio of (O+N)/C, O/C and H/C ranged from 0.26 to 0.48, 0.26 to 0.48 and 0.05 to 0.09, while the respective ratios of biochar produced at 700 °C ranged from 0.08 to 0.09 and 0.07 to 0.08, and were 0.02 [16,19,61].

The transformation of agricultural biomass during pyrolysis alters the molecular structures of biochar in various ways [20] and further modifies its properties through thermal degradation of easily decomposable oxygen-containing molecular structures [20,21]. With an increase in PT, the ash content increased from 8.8 (B-400) to 11.6% (B-700), and the EC increased from 0.21 to 0.53 dS m^{-1} (Tables S1 and S2). The ash content of biochar increased due to the release of volatiles [53], while the EC increased as a result of non-volatiles remaining after pyrolysis [54]. Therefore, the ash content indicates the concentration of inorganic constituents, while the EC represents total concentration of dissolved salts or total amount of dissolved ions resulting from thermal decomposition of agricultural biomass [8,9]. From those relations, we infer that inorganic and alkali salts that were combined with the volatile biomass structures containing C, H, O, and N began to separate from the agricultural biochar feedstocks, and that more nonvolatile inorganic and alkali salts were deposited more in B-700 during thermal decomposition [10,11]. As more alkali salts were deposited at higher PT, the pH of B-700 (10.5) was higher than that of B-400 (9.0). Since solution-pH determines the net surface charge of the sorbent, biochar can have positively and negatively charged surfaces for hydrophilic interactions at a given pH [55]. This means that the net surface charge of B-400 and B-700 is positive at circumneutral pH, with more positive charges at the surface of the latter [56].

The acidity of B-400 and B-700 was measured at 0.150 and 0.013 mmol g^{-1} for carboxylic acid groups, 0.167 and 0.125 mmol g^{-1} for lactonic acid groups, and 0.421 and 0.013 mmol g^{-1} for phenolic acid groups, respectively, as observed in our previous study [56], and the decrease in the acidity of surface functional groups with increasing PT was due to volatilization of oxygen-containing structures [15,64]. The results of XRF spectra confirmed more deposition of inorganic salts in B-700 than in B-400 (Table S2). Concentration of Si was 1.61% for B-400 and 2.35% for B-700, as a result of Si-accumulation due to pyrolysis, which was higher than that of biochar feedstock (0.60%). However, concentrations of K, Ca, P, Mg, S, Al and Fe in both biochar were below 1%.

2. SCD of Biochar

The positive SCD of *Miscanthus* biochar decreased from 0.08 to −0.06 C m^{-2} for B-400 and from 0.05 to −0.01 C m^{-2} for B-700 as pH increased (Fig. 1). The positive biochar SCD was associated with the concentration of oxygen-containing AFGs; progressive thermal decomposition caused polarization and hydrophilization of biochar [57,58], resulting in a decreased proportion of AFGs and SCD in B-700 (Table S1).

In both B-400 and B-700, the SCD remarkably decreased at pH values of 4 to 5, 7 to 8, and above 10 (Fig. 1), which corresponded to the pK_a values of carboxylic (pK_a=4-5), lactonic (pK_a=7-8) and phenolic (pK_a=10) functional groups, respectively [23]. However, a decrease in SCD of biochar was also observed in the pH range between 2 and 3, in which the pK_a values of surface AFGs are not applicable; this decrease could be explained by the interaction of deposited alkali salts with H^+ ions in solution, leading to electrostatic stabilization [59,60]. Kloss et al. and Tran et al. reported that the positive SCD of biochar decreased with increasing pH and that the decreasing effect was diminished with increasing PT as a

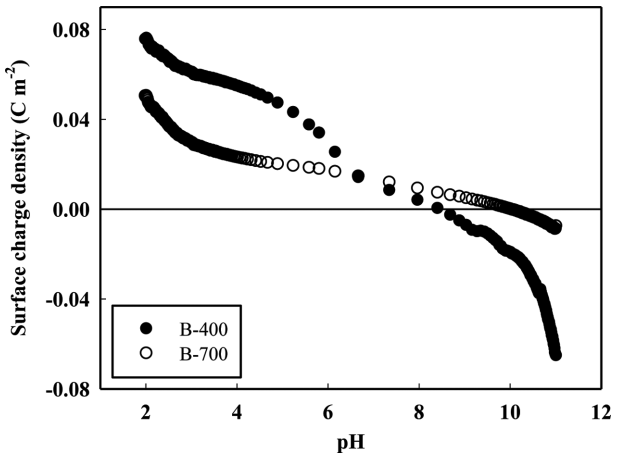

Fig. 1. Surface charge density (SCD) of *Miscanthus* biochar produced at two pyrolysis temperatures of 400 °C (B-400) and 700 °C (B-700) as a function of pH determined by potentiometric titration in 0.05 M $CaCl_2$ solution.

result of a reduction in deprotonated surface AFGs, which reduced polarization and hydrophilization [61,62]. Therefore, we believe that deprotonation of AFGs and deposition of alkali salts on the surface of biochar are the main causes of the reduction in SCD with increasing pH [59,61]. Thus, a greater reduction in the positive SCD of biochar at higher pH values was due to a progressive deprotonation of biochar AFGs in pH ranges that include the pK_a values of surface AFGs (Table S1) and to enhanced deposition of inorganic and alkali salts on the biochar (Table S2).

3. Effect of pH and CV in Background Electrolyte Solutions on Simazine Sorption

The sorption isotherms constructed at pH values of 3.5, 7.5 and 10 under different background electrolyte conditions were fitted to the Langmuir and Freundlich isotherms (Fig. 2), and the fitting results indicated that the Freundlich model yielded a better fit of simazine sorption to biochar than the Langmuir model, as was evident from higher mean R^2 and lower mean Δq on the fitted parameters (Table 1). Yuan et al. showed that the Freundlich model well described the alteration in SCD due to protonation and/or deprotonation of AFGs on biochar surface in the sorption process of carbaryl and atrazine [12,63]. Sun et al. reported that the interaction of fluridone with biochar was altered by changes in pH due to the alteration in the SCD of biochar, which affects the sorption mechanism in terms of H-bonding and/or van der Waals forces [64]. Therefore, we interpreted the pH-dependent sorption mechanism of simazine on biochar in terms of the PCs of biochar, since electrostatic interactions between H-bonding and hydrophobic interactions such as van der Waals forces and pore-filling mechanisms create heterogeneity in biochar [36].

As pH increased from 3.5 to 10, the constant K_F decreased from

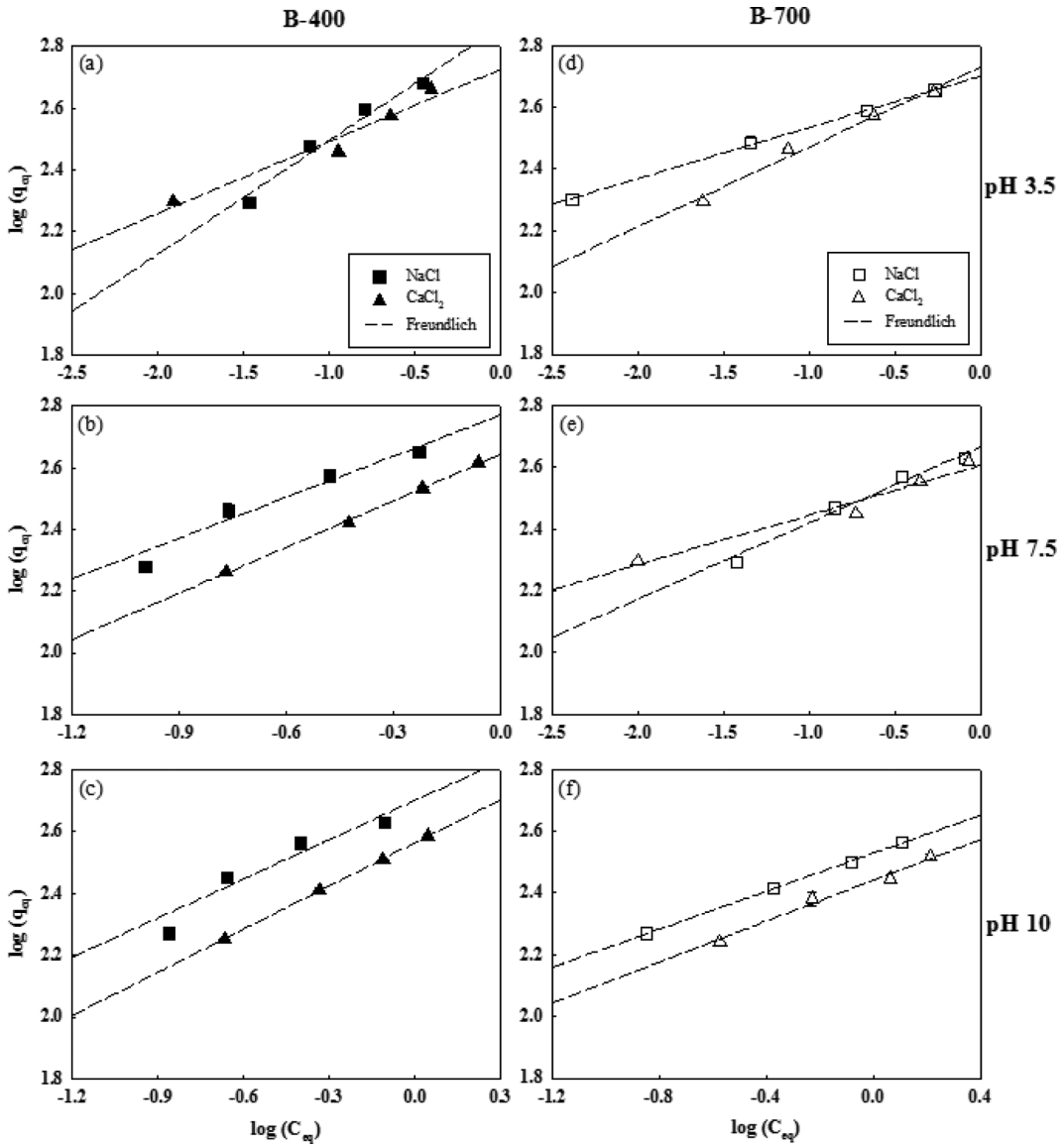

Fig. 2. Simazine sorption isotherms fitted to the linear Freundlich model in 0.1 M NaCl (rectangles) and 0.05 M $CaCl_2$ (triangles) for B-400 ((a)-(c), indicated on the left side with solid symbols) and B-700 ((d)-(f), indicated on the right side with open symbols) at three pH values of 3.5, 7.5 and 10. The mixture was agitated at 160 rpm for 81 h at room temperature of 25±0.5 °C.

Table 1. Linear Freundlich and Langmuir sorption isotherm parameters for simazine sorption on *Miscanthus* biochar produced at two pyrolysis temperatures of 400 °C (B-400) and 700 °C (B-700) obtained at three pH values in 0.1 M NaCl and 0.05 M $CaCl_2$ solutions, with the results of two-way analysis of variance (ANOVA) showing the significance of the effects of two factors and their interaction on each isotherm parameter. The mixture was shaken at 160 rpm for 81 h at 25±0.5 °C

			Linear Freundlich isotherm				Langmuir isotherm			
Biochar	Cation valence	pH	$\log K_F$	1/n	R^2	Δq	K_L	q_{max}	R^2	Δq
B-400	Na^+	3.5	2.81 (0.03)	0.36 (0.03)	0.96	1.6	14.7 (1.2)	565.6 (15.7)	0.99	4.5
		7.5	2.77 (0.03)	0.44 (0.04)	0.94	1.5	5.2 (0.5)	593.3 (22.9)	0.99	6.1
		10	2.70 (0.03)	0.42 (0.05)	0.91	1.7	4.4 (0.5)	557.4 (3.90)	0.98	6.1
	Ca^{2+}	3.5	2.73 (0.02)	0.23 (0.02)	0.96	1.9	46.0 (20.3)	423.3 (33.6)	0.76	23.3
		7.5	2.64 (0.00)	0.50 (0.01)	1.00	1.1	2.2 (0.3)	615.6 (36.2)	0.98	8.5
		10	2.56 (0.00)	0.47 (0.01)	1.00	0.3	1.9 (0.2)	552.2 (27.4)	0.98	4.5
ANOVA										
Cation valence			***	n.s.			n.s.	n.s.		
pH			***	**			n.s.	**		
Cation valence x pH			n.s.	n.s.			n.s.	**		
B-700	Na^+	3.5	2.70 (0.02)	0.17 (0.01)	0.99	0.4	137.0 (53.6)	413.1 (25.3)	0.75	15.6
		7.5	2.67 (0.01)	0.25 (0.02)	0.97	0.8	16.2 (2.3)	444.2 (14.8)	0.96	6.9
		10	2.53 (0.00)	0.31 (0.00)	1.00	0.3	4.5 (0.7)	413.5 (18.9)	0.98	6.6
	Ca^{2+}	3.5	2.73 (0.02)	0.26 (0.01)	0.99	1.0	27.2 (3.7)	453.5 (14.6)	0.97	8.8
		7.5	2.60 (0.01)	0.16 (0.01)	0.96	1.6	73.9 (23.3)	368.1 (17.3)	0.75	24.7
		10	2.44 (0.01)	0.33 (0.02)	0.97	1.1	2.8 (0.5)	384.8 (18.7)	0.94	6.8
ANOVA										
Cation valence			**	n.s.			n.s.	n.s.		
pH			***	**			n.s.	n.s.		
Cation valence x pH			**	*			n.s.	n.s.		

***: Significant at $p<0.001$ level; **: Significant at $p<0.01$ level; *: Significant at $p<0.05$ level; n.s.: not significant ($p>0.05$).

645.7 to 501.2 in 0.1 M NaCl solution (ionic strength=0.1) and from 537.0 to 363.1 in 0.1 M $CaCl_2$ solution (ionic strength=0.15) for B-400, while their counterparts for B-700 decreased from 501.2 to 338.8 and from 537.0 to 275.4, respectively (Table 1). A decrease in K_F with increasing pH could be explained by the decrease in sorption strength between sorbate and sorbent [65], since an increase in the negativity of the SCD of biochar due to progressive deprotonation of AFGs at a pH above 1.7 (the pK_a of simazine) [28] increases electrostatic repulsion with neutral simazine molecules [18,66]. Wang and Lemley observed a decrease in the sorption strength of ametryn to soil with increasing pH due to enhanced electrostatic repulsion (lower K_F) [65], and Rajapaksha et al. demonstrated that K_F (a proxy of sorption capacity) of sulfamethazine sorption decreased with increasing pH as electrostatic repulsion increased [47].

Even though lower K_F was expected for B-400 due to its lower SSA and to more deprotonation at the surface (Table S1), K_F of B-700 for simazine sorption was invariably lower than the corresponding value of B-400 at a given pH and CV, indicating that CV-driven alterations in pore space morphology may predominate over pH-driven deprotonation of AFGs at the surface acidic sites. Therefore, we inferred that the reduction of simazine sorption can be predominantly attributed to greater blocking of the entrance to internal pores due to the formation of larger metal-biochar complexes [67,68], even though progressive deprotonation with increasing pH increases electrostatic repulsion between neutral simazine molecules and biochar [69,70]. In addition, decreases in K_F with increasing pH were greater in Ca^{2+} electrolyte than in Na^+ electrolyte for both B-400 and B-700 (Table 1), indicating that Ca^{2+} ions compete with simazine molecules to a greater extent for the binding sites of biochar than Na^+ ions. Changing CV from Na^+ to Ca^{2+} caused the formation of larger metal-biochar complexes that blocks to a greater extent the entrance of internal pores (Fig. 3).

An increase in CV resulted in a decrease in K_F of biochar at a given pH and PT, with a greater decrease at higher pH values (Table 1). However, CV-driven changing patterns of K_F with pH were different between B-400 and B-700. The patterns of decreasing K_F with increasing pH were parallel under both electrolyte conditions for B-400; however, the two patterns crossed at the middle pH (7.5) for B-700, indicating a significant interactive effect of pH and CV on K_F for B-700 (Fig. 2). The K_F values of B-700 in Ca^{2+} solution were higher at pH 3.5 and lower at pH 10 than their counterparts in Na^+ solution. On the other hand, pH affected the strength of simazine sorption (1/n) while CV did not. However, a significant interaction between pH and CV was observed for B-700 but not for B-400 (Table 1). Lee et al. identified that at least two dominant sorption mechanisms of simazine occur at multiple types of binding sites on biochar: a strong sorption process due

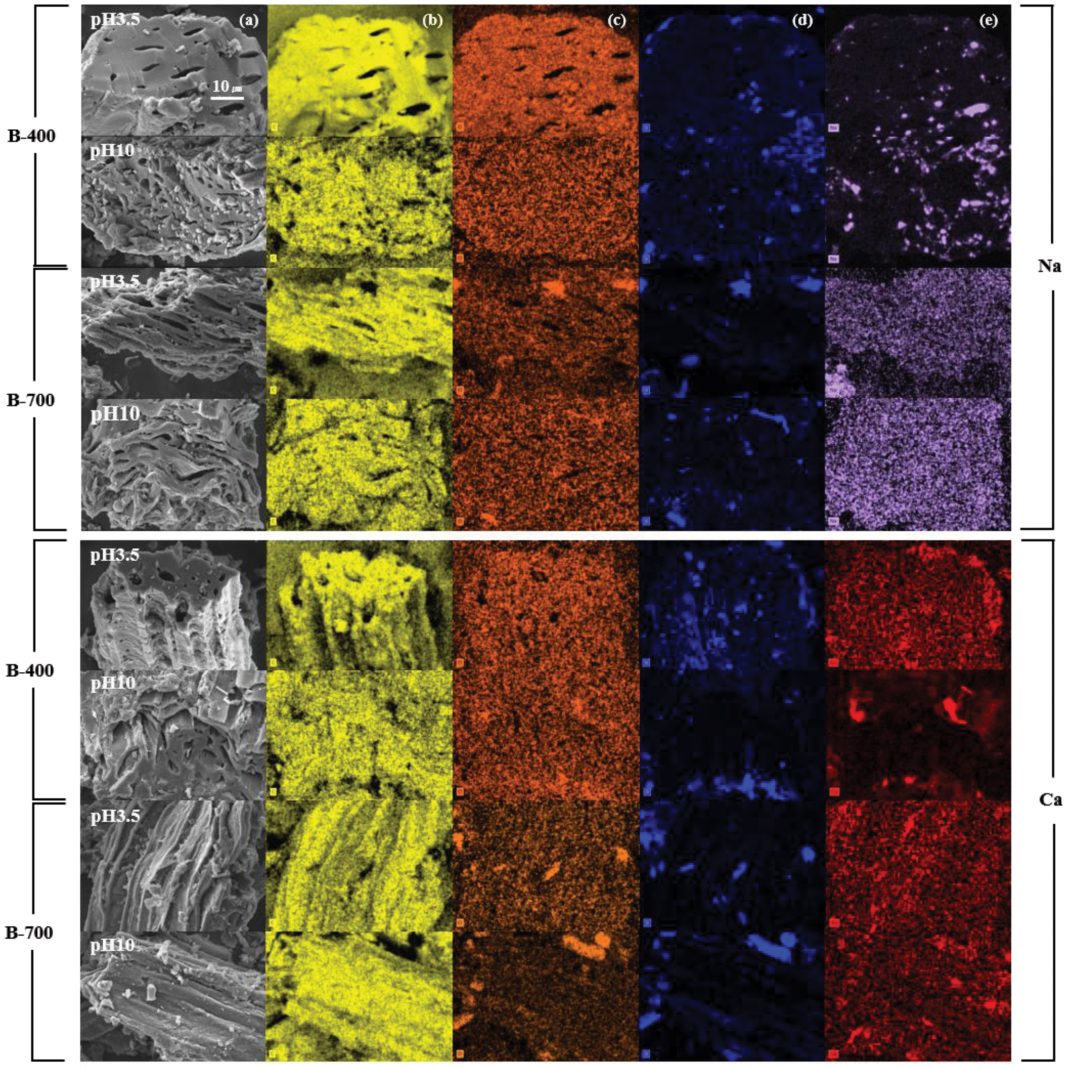

Fig. 3. FE-SEM/EDS images of (a) morphology (black), (b) C (yellow), (c) O (orange), (d) Si (blue), and (e) Na (purple) or Ca (red) for two types of biochar produced at 400 and 700 °C (B-400 and B-700, respectively), obtained after simazine sorption at pH 3.5 and 10 in 0.1 M NaCl or 0.05 M $CaCl_2$ solutions.

to electrostatic attraction in the lower sorption range and a weak sorption process *via* hydrophobic attraction in the higher sorption range [56].

Overall, an increase in CV lowered K_F, and the corresponding decrease at a given pH was greater for B-700 than for B-400. This phenomenon can be explained by the formation of larger metal-biochar complexes (Fig. 3) that blocks to a greater extent the entrances of the intramolecular pore spaces available for simazine sorption [67,68] at more deprotonated (negatively charged) acidic sites on biochar (Table S1) [26]. Previous studies have shown that the PCs of a sorbent are altered by changing the background electrolyte ions. Largeot et al. demonstrated that the size (hydrated radius) of the background electrolyte changed the pore size of biochar-derived carbon by affecting the formation of metal complexes [71], and Gabelich et al. showed that the effective SSA of clay available for sorption was lower than that measured by using BET analysis due to the interactions of carbon with background electrolyte ions [72]. We could infer then that environmental factors such as pH and CV in background electrolyte solutions affect the strength and mechanism of simazine sorption at the surface of biochar by altering the PCs of biochar. Therefore, we concluded that progressive deprotonation of AFGs on the surface of biochar with increasing pH and the blockage of biochar intra-pores by the deposition of metal complexes due to increasing CV may be the main mechanism for a decrease in K_F in response to increasing pH and CV in background electrolytes.

4. Effect of Pore Structure of Biochar on Simazine Sorption

As pH increased from 3.5 to 10, the deposition of Na^+ or Ca^{2+} on the surface of biochar increased for the two types of biochar (Fig. 3); the concentrations of the relevant ions increased from 0.67 to 3.69 in NaCl solution and 0.41 to 1.56 in $CaCl_2$ solution for B-400 and from 0.24 to 0.56 and 0.29 to 0.54 for B-700 in the corresponding electrolyte solutions, respectively (Table S3). An increase in Na^+ or Ca^{2+} on the surface of biochar can interrupt the sorption of simazine due to the formation of metal-biochar complexes, since negative surface charge developed from progressive

deprotonation of AFGs interact with cations in electrolyte solutions. This causes the blocking of the pore spaces available for simazine sorption in response to increasing pH and CV in the background electrolyte solution, resulting in different sizes of hydrated radii in the ionic atmosphere of the solution [73,74]. The SEM morphology images showed the accumulation of Na^+ or Ca^{2+} on the biochar surface to a greater extent with increasing pH and CV (Fig. 3). In particular, the amount of simazine sorbed on biochar was higher in Na^+ electrolyte solution than in Ca^{2+} electrolyte solution (Fig. 2).

Despite higher deposition of Na^+ or Ca^{2+} on B-400 than on B-700 (Fig. 3), since the formation of metal-biochar complexes was greater in B-400 than in B-700 due to higher concentration of AFGs on the surface, the sorption of simazine was also greater in B-400 (Fig. 2). This relationship can be explained by the fact that the pores of B-700, which had more large pores available for simazine sorption (Table S1), were more blocked than those of B-400, as a result of increased pore-filling mechanism [75]. For this reason, less simazine was sorbed on B-700 than on B-400 despite its higher SSA (Table S1). Therefore, we confirmed that the amount of simazine sorbed on biochar is a function of altered PCs of biochar under varying pH and CV conditions in a background electrolyte solution. Under circumneutral pH regions in soil-water systems, the neutral species of simazine may bind mainly to the hydrophobic sorption sites of biochar through van der Waals forces and the pore-filling mechanisms; however, it can bind to its hydrophilic sorption sites through intermolecular interactions such as H-bonding (a relatively minor mechanism) [76].

5. Environmental Effects of Biochar on Ionizable Organic Pollutant Remediation

In general, the sorption of ionizable organic pollutants to biochar involves three possible mechanisms: π-π electron donor-acceptor (EDA) interactions, van der Waals forces, and weak H-bonding [76,77]. EDA interactions describe the binding of electron-donor molecules (organic pollutants) to electron-acceptor sites (aromatic C in biochar) [12], while H-bonding occurs between positively charged organic pollutants and the negatively charged surface of biochar [12], and van der Waals forces involve the binding of sorbate molecules to biochar without covalent or ionic bonding [78]. In our previous study, we found that two types of biochar binding sites responded independently to changing pH and/or PT: strong sorption occurred in the lower sorption range due to EDA and/or H-bonding interactions, and relatively weak sorption occurred in the higher sorption range due to van der Waals forces [56].

However, the relative contribution of each of these mechanisms to the sorption of ionizable organic pollutants, such as simazine, to biochar varies with environmental factors such as pH and CV in the background electrolyte solution, since these factors alter the PCs and SCD of biochar and ionizable organic molecules, as observed in this study. Therefore, we can explain the mechanisms for simazine sorption to biochar in terms of pH and CV and their interactions. Under the acidic pH conditions below its PZNC, the positively charged surface of biochar interacts with neutral simazine molecules *via* H-bonding, van der Waals forces and the pore-filling mechanism. However, an increase in pH causes more electrostatic repulsion of neutral simazine due to more deprotonation of AFGs at respective pK_a. On the other hand, changing to a higher CV in a background electrolyte solution can lead to greater blocking of the entrance to intra-structural pores due to the formation of larger metal-biochar complexes. Therefore, we observed decreased sorption capacity (K_F) of biochar for simazine in both B-400 and B-700 as pH and CV increased (Table 1) due to increased repulsive van der Waals forces and pore-filling mechanism.

As pH and CV of the surrounding electrolytic solution affect the morphological and physicochemical characteristics of biochar, we presumed that the behavior of simazine sorption to biochar and the relative contribution of each factor and their interactions to K_F of biochar for simazine were different between B-400 and B-700. In this study, we also found that K_F of biochar was invariably lower in B-700 than in B-400 at any combination of the levels of two factors (Table 1), even though the former had higher SSA and lower AFGs than the latter (Table S1). Besides, even though greater decreases in K_F for simazine were expected for B-400 due to more deprotonation at the surface acidic sites and to its lower SSA, the entire sorption capacity (K_F) was lower in B-700. From these relations, we can deduce that CV-driven pore-filling mechanisms dominate over pH-driven repulsive van der Waals forces in controlling the sorption affinity and capacity of biochar for simazine, when pH and CV are concerned.

Therefore, we believe that the PCs of biochar should be considered in order to effectively control ionizable organic pollutants that are positively, negatively or neutrally charged depending on protonation or deprotonation [24,79]. For example, the negatively charged surface of biochar due to progressive deprotonation of surface AFGs with increasing pH above its PZNC attracts cation species or positively charged ionizable organic pollutants to achieve electrostatic stabilization, but repulses negatively or neutrally charged ionizable organic pollutants through electrostatic repulsion [16,24, 66]. In addition, our results clearly revealed that CV of the background electrolyte solution is another key factor affecting the pH-dependent sorption of ionizable organic molecules to a variable-charge sorbent. Thus, an understanding of the PCs and charge behavior of biochar and ionizable organic pollutants under various environmental conditions is a prerequisite to assessing the efficacy of remediation and its environmental risks in real environments such as soils and nearby waters.

CONCLUSIONS

We hypothesized that pH and CV in a background electrolyte solution would determine the behavior of the sorption of simazine (containing lone-pair electrons) to biochar (carrying variable SCD) by altering the charge behavior and surface morphology of biochar, and the sorption response would be different depending on PT because PT governs pore space morphology and surface charge behavior of biochar. We tested this hypothesis by interpreting the effects of pH, CV and their interactions on PT-driven simazine sorption. Fitting of experimental data of simazine sorption to the Freundlich model obviously showed that K_F of biochar for simazine decreased as pH and CV increased due, respectively, to increased electrostatic repulsion for neutral simazine molecules with increasing pH and, predominantly, to more inhibition of internal pore

entrances with increasing CV. The pH-driven decreases in K_F were greater with Ca^{2+} ions (higher CV), while CV-driven decreases were greater at higher pH values. However, we also observed invariably lower K_F of biochar in B-700 than in B-400 at any given combination of the levels of pH and CV, even though higher K_F was expected for the former from its higher SSA and lower AFGs at the surface. This discrepancy means that increasing CV contributes to a greater extent to decreased K_F than increasing pH. From these relations, we deduced that CV-driven alterations in pore space and surface morphology predominate over pH-driven van der Waals forces in controlling the sorption affinity and capacity of biochar for simazine, where pH and CV are concerned. The results confirmed our hypothesis by revealing that changing CV alters the surface coverage available for simazine sorption and the blocking of the entrance to internal pore space, while pH governs protonation/deprotonation of AFGs, and that CV predominates over pH in controlling the behavior of simazine (containing lone-pair electrons) sorption to biochar (carrying variable SCD). Therefore, we believe that our approach and findings will contribute to a more comprehensive understanding of the sorption mechanisms and behavior of ionizable organic pollutants (variable-charge sorbates) to the surface of biochar (variable-charge sorbent) and help better interpret their environmental occurrence, behavior, transport and fate under natural soils and nearby water environments.

ACKNOWLEDGEMENTS

This research was supported by the Basic Science Research Program through the National Research Foundation of Korea (NRF) (NRF-2016R1D1A1B03934038) and by the Brain Korea 21 PLUS program, funded by the Ministry of Education of Korea.

SUPPORTING INFORMATION

Additional information as noted in the text. This information is available via the Internet at http://www.springer.com/chemistry/journal/11814.

REFERENCES

1. Y. Qiu, Z. Zheng, Z. Zhou and G. D. Sheng, *Bioresour. Technol.*, **100**, 5348 (2009).
2. J. Lehmann, *Nature*, **447**, 143 (2007).
3. A. Zielińska, P. Oleszczuk, B. Charmas, J. Skubiszewska-Zięba and S. Pasieczna-Patkowska, *J. Anal. Appl. Pyrolysis*, **112**, 201 (2015).
4. L. Zhao, X. Cao, O. Mašek and A. Zimmerman, *J. Hazard. Mater.*, **256-257**, 1 (2013).
5. T. Mimmo, P. Panzacchi, M. Baratieri, C. A. Davies and G. Tonon, *Biomass Bioenergy*, **62**, 149 (2014).
6. T. Qu, W. Guo, L. Shen, J. Xiao and K. Zhao, *Ind. Eng. Chem. Res.*, **50**, 10424 (2011).
7. Y. Elmay, Y. Le Brech, L. Delmotte, A. Dufour, N. Brosse and R. Gadiou, *J. Anal. Appl. Pyrolysis*, **113**, 402 (2015).
8. R. R. Domingues, P. F. Trugilho, C. A. Silva, I. C. N. A. De Melo, L. C. A. Melo, Z. M. Magriotis and M. A. Sánchez-Monedero, *PLoS One*, **12**, 1 (2017).
9. D. Angin, *Bioresour. Technol.*, **128**, 593 (2013).
10. A. Méndez, M. Terradillos and G. Gascó, *J. Anal. Appl. Pyrolysis*, **102**, 124 (2013).
11. X. Cao and W. Harris, *Bioresour. Technol.*, **101**, 5222 (2010).
12. X. Zhang, H. Wang, L. He, K. Lu, A. Sarmah, J. Li, N. S. Bolan, J. Pei and H. Huang, *Environ. Sci. Pollut. Res.*, **20**, 8472 (2013).
13. J. Tang, W. Zhu, R. Kookana and A. Katayama, *J. Biosci. Bioeng.*, **116**, 653 (2013).
14. P. Cely, A. M. Tarquis, J. Paz-Ferreiro, A. Méndez and G. Gascó, *Solid Earth.*, **5**, 585 (2014).
15. K. G. I. D. Kumari, P. Moldrup, M. Paradelo and L. W. De Jonge, *Water. Air. Soil Pollut.*, **225**, 2015 (2014).
16. F. Lian, B. Sun, Z. Song, L. Zhu, X. Qi and B. Xing, *Chem. Eng. J.*, **248**, 128 (2014).
17. W. Zheng, M. Guo, T. Chow, D. N. Bennett and N. Rajagopalan, *J. Hazard. Mater.*, **181**, 121 (2010).
18. M. Uchimiya, S. C. Chang and K. T. Klasson, *J. Hazard. Mater.*, **190**, 432 (2011).
19. T. M. Vu, V. T. Trinh, D. P. Doan, H. T. Van, T. V. Nguyen, S. Vigneswaran and H. H. Ngo, *Sci. Total Environ.*, **579**, 612 (2017).
20. H. P. Boehm, *Carbon N.Y.*, **32**, 759 (1994).
21. Z. Reddad, C. Gerente, Y. Andres and P. Le Cloirec, *Environ. Sci. Technol.*, **36**, 2067 (2002).
22. M. S. Rahman and M. R. Islam, *Chem. Eng. J.*, **149**, 273 (2009).
23. C. A. Leon and L. R. Radovic, *Mater. Sci.*, **202**, 1007 (1991).
24. J. J. Pignatello, J. Z. Ni and B. S. Xing, *Abstr. Pap. Am. Chem. Soc.*, **242**, 9240 (2011).
25. F. Qi, Y. Yan, D. Lamb, R. Naidu, N. S. Bolan, Y. Liu, Y. S. Ok, S. W. Donne and K. T. Semple, *Bioresour. Technol.*, **246**, 48 (2017).
26. X. Dong, L. Q. Ma and Y. Li, *J. Hazard. Mater.*, **190**, 909 (2011).
27. H. Zheng, Z. Wang, J. Zhao, S. Herbert and B. Xing, *Environ. Pollut.*, **181**, 60 (2013).
28. M. Chen, D. Wang, F. Yang, X. Xu, N. Xu and X. Cao, *Environ. Pollut.*, **230**, 540 (2017).
29. M. Silva and P. Iyer, *Birth Defects Res. Part B - Dev. Reprod. Toxicol.*, **101**, 308 (2014).
30. A. S. Gunasekara, J. Troiano, K. S. Goh and R. S. Tjeerdema, *Rev. Environ. Contam. Toxicol.*, **189**, 1 (2007).
31. S. V. Trentacoste, A. S. Friedmann, R. T. Youker, C. B. Breckenridge and B. R. Zirkin, *J. Androl.*, **22**, 142 (2001).
32. USEPA, *Triazine cumulative risk assessment*, Washington D.C. USGPO (2006).
33. J. B. Weber, *Soil Sci. Soc. Am. J.*, **34**, 401 (2010).
34. B. Chen, D. Zhou and L. Zhu, *Environ. Sci. Technol.*, **42**, 5137 (2008).
35. J. Lehmann, *Front. Ecol. Environ.*, **5**, 381 (2007).
36. G. Zhang, Q. Zhang, K. Sun, X. Liu, W. Zheng and Y. Zhao, *Environ. Pollut.*, **159**, 2594 (2011).
37. G. Sigmund, T. Hüffer, T. Hofmann and M. Kah, *Sci. Total Environ.*, **580**, 770 (2017).
38. A. Mukherjee, A. R. Zimmerman and W. Harris, *Geoderma*, **163**, 247 (2011).
39. J. Wang, H. Liu, S. Yang, J. Zhang, C. Zhang and H. Wu, *Appl. Surf. Sci.*, **316**, 443 (2014).
40. A. Contescu, C. Contescu, K. Putyera and J. A. Schwarz, *Carbon N.Y.*, **35**, 83 (1997).
41. P. Zhang, H. Sun, L. Yu and T. Sun, *J. Hazard. Mater.*, **244-245**,

217 (2013).
42. S. Rajkovich, A. Enders, K. Hanley, C. Hyland, A. R. Zimmerman and J. Lehmann, *Biol. Fertil. Soils.*, **48**, 271 (2012).
43. Y. Yang, Y. Chun, G. Shang and M. Huang, *Langmuir*, **20**, 6736 (2004).
44. M. Szekeres and E. Tombácz, *Colloids Surf. A Physicochem. Eng. Asp.*, **414**, 302 (2012).
45. USEPA, *Fate, transport and transformation test guidelines*, Washington D.C. USGPO (1998).
46. V. Morgante, C. Flores, X. Fadic, M. González, M. Hernández, F. Cereceda-Balic and M. Seeger, *J. Environ. Manage.*, **95**, S300 (2012).
47. A. U. Rajapaksha, M. Vithanage, M. Ahmad, D. C. Seo, J. S. Cho, S. E. Lee, S. S. Lee and Y. S. Ok, *J. Hazard. Mater.*, **290**, 43 (2015).
48. L. M. Cozmuta, A. M. Cozmuta, A. Peter, C. Nicula, E. Bakatula Nsimba and H. Tutu, *Water SA.*, **38**, 269 (2012).
49. A. M. El-Kamash, A. A. Zaki and M. A. El Geleel, *J. Hazard. Mater.*, **127**, 211 (2005).
50. A. Zielińska and P. Oleszczuk, *Bioresour. Technol.*, **192**, 618 (2015).
51. G. Abdul, X. Zhu and B. Chen, *Chem. Eng. J.*, **319**, 9 (2017).
52. L. Han, L. Qian, J. Yan and M. Chen, *Chemosphere*, **156**, 262 (2016).
53. Y. Wang, L. Qiu, M. Zhu, G. Sun, T. Zhang and K. Kang, *Sci. Rep.*, **9**, 1 (2019).
54. C. Gai, Y. Li, N. Peng, A. Fan and Z. Liu, *Bioresour. Technol.*, **185**, 240 (2015).
55. A. Silber, I. Levkovitch and E. R. Graber, *Environ. Sci. Technol.*, **44**, 9318 (2010).
56. S. Lee, J. Han and H. M. Ro, *Korean J. Chem. Eng.*, **35**, 1468 (2018).
57. F. Xiao and J. J. Pignatello, *Environ. Sci. Technol.*, **50**, 6276 (2016).
58. M. Essandoh, B. Kunwar, C. U. Pittman, D. Mohan and T. Mlsna, *Chem. Eng. J.*, **265**, 219 (2015).
59. X. Li, L. Jiang, L. Li and Y. Yan, *J. Mater. Sci.*, **52**, 4367 (2017).
60. K. Ruthenberg and H. Chang, *Stud. Hist. Philos. Sci. Part A.*, **65-66**, 121 (2017).
61. S. Kloss, F. Zehetner, A. Dellantonio, R. Hamid, F. Ottner, V. Liedtke, M. Schwanninger, M. H. Gerzabek and G. Soja, *J. Environ. Qual.*, **41**, 990 (2012).
62. H. N. Tran, S. J. You and H. P. Chao, *Korean J. Chem. Eng.*, **34**, 1708 (2017).
63. J. H. Yuan, R. K. Xu and H. Zhang, *Bioresour. Technol.*, **102**, 3488 (2011).
64. K. Sun, M. Keiluweit, M. Kleber, Z. Pan and B. Xing, *Bioresour. Technol.*, **102**, 9897 (2011).
65. Q. Wang and A. T. Lemley, *J. Environ. Sci. Heal. - Part B Pestic. Food Contam. Agric. Wastes*, **41**, 223 (2006).
66. Q. Fang, B. Chen, Y. Lin and Y. Guan, *Environ. Sci. Technol.*, **48**, 279 (2014).
67. S. Narasimha Rao and P. K. Mathew, *Clays Clay Miner.*, **43**, 433 (1995).
68. I. Persson, *Pure Appl. Chem.*, **82**, 1901 (2010).
69. P. Peng, Y. H. Lang and X. M. Wang, *Ecol. Eng.*, **90**, 225 (2016).
70. E. Kim, C. Jung, J. Han, N. Her, C. M. Park, M. Jang, A. Son and Y. Yoon, *J. Ind. Eng. Chem.*, **36**, 364 (2016).
71. C. Largeot, C. Portet, J. Chmiola, P. L. Taberna, Y. Gogotsi and P. Simon, *J. Am. Chem. Soc.*, **130**, 2730 (2008).
72. C. J. Gabelich, T. D. Tran and I. H. M. Suffet, *Environ. Sci. Technol.*, **36**, 3010 (2002).
73. T. H. Nguyen, H. H. Cho, D. L. Poster and W. P. Ball, *Environ. Sci. Technol.*, **41**, 1212 (2007).
74. M. R. Powell, L. Cleary, M. Davenport, K. J. Shea and Z. S. Siwy, *Nat. Nanotechnol.*, **6**, 798 (2011).
75. L. Borchardt, M. Oschatz, S. Paasch, S. Kaskel and E. Brunner, *Phys. Chem. Chem. Phys.*, **15**, 15177 (2013).
76. U. Herwig, E. Klumpp, H. D. Narres and M. J. Schwuger, *Appl. Clay Sci.*, **18**, 211 (2001).
77. D. Zhu, S. Hyun, J. J. Pignatello and L. S. Lee, *Environ. Sci. Technol.*, **38**, 4361 (2004).
78. W. Liu, J. Carrasco, B. Santra, A. Michaelides, M. Scheffler and A. Tkatchenko, *Phys. Rev. B - Condens. Matter Mater. Phys.*, **86**, 1 (2012).
79. D. J. de Ridder, L. Villacorte, A. R. D. Verliefde, J. Q. J. C. Verberk, S. G. J. Heijman, G. L. Amy and J. C. van Dijk, *Water Res.*, **44**, 3077 (2010).

Supporting Information

Interactive effect of pH and cation valence in background electrolyte solutions on simazine sorption to *Miscanthus* biochar produced at two different pyrolysis temperatures

Seoyeon Lee, Junho Han, and Hee-Myong Ro†

Department of Agricultural Biotechnology and Research Institute of Agriculture and Life Sciences, Seoul National University, Seoul 08826, Korea
(*Received 9 September 2019 • accepted 21 December 2019*)

Table S1. Physicochemical characteristics of *Miscanthus* biochar pyrolyzed at two temperatures of 400 °C (B-400) and 700 °C (B-700)

Biochar	Specific surface area[a] ($m^2\ g^{-1}$)		Elemental composition[c] (%)					Atomic ratio[c]			Acidic functional groups[d] (mmol g^{-1})[d]			Ash[e] %	EC[f] (dS m^{-1})	pH[f]	PZNC[g]
	Micro-pores[b]	Nano-pores[b]	C	H	O	N	S	(O+N)/C	H/C	O/C	Carboxylic	Lactonic	Phenolic				
B-400	5.6	191.6	70.5	3.5	25.3	0.6	0.02	0.37	0.05	0.36	0.150	0.167	0.421	8.80	0.21	9.0	8.84
B-700	236.3	57.2	79.2	1.1	19.2	0.4	0.02	0.25	0.01	0.24	0.013	0.125	0.013	11.6	0.53	10.5	10.0

[a]Specific surface area (SSA) was estimated based on the results obtained from BET isotherms using N_2 (N_2-BET) and CO_2 (CO_2-BET).
[b]The SSA of micropores was equal to the N_2-BET results, while that of nanopores was calculated by subtracting the CO_2-BET results from the N_2-BET results.
[c]Elemental composition was measured using an elemental analyzer, and the atomic ratio was calculated.
[d]Acidic functional groups were measured by Boehm titration.
[e]Ash content was estimated by the combustion method.
[f]EC and pH were measured with an EC meter and a pH meter, respectively.
[g]The point of zero net charge (PZNC) was estimated by the pH drift method.

Table S2. XRF results of dried *Miscanthus* and biochar pyrolyzed at two temperatures of 400 °C (B-400) and 700 °C (B-700)

Components	Dried *Miscanthus*	B-400	B-700
	Mass percent (%)		
CH_2	99.9	97.0	95.7
Si	0.60	1.61	2.35
K	0.05	0.68	0.98
Ca	0.11	0.22	0.30
P	0.04	0.17	0.23
Mg	0.05	0.15	0.22
S	0.02	0.04	0.05
Al	0.01	0.03	0.05
Fe	0.01	0.02	0.03
Cl	0.08	0.02	0.06
Mn	0.01	0.02	0.02
Zn	0.00	0.00	0.01

Table S3. FE-SEM/EDS elemental analysis results for two types of biochar produced at 400 and 700 °C (B-400 and B-700) obtained after simazine sorption at pH 3.5 and 10 in 0.1 M NaCl or 0.05 M $CaCl_2$ solutions

			Elemental concentration (%)			
Biochar	Cation valence	pH	C	O	Si	Na^+ or Ca^{2+}
B-400	Na^+	3.5	73.08±22.42	24.01±8.05	2.24±0.14	0.67±0.19
		10	68.32±21.41	23.34±8.46	4.65±0.14	3.69±0.72
	Ca^{2+}	3.5	72.88±22.69	25.30±9.03	1.41±0.19	0.41±0.12
		10	69.02±21.41	27.65±9.59	1.77±0.17	1.56±0.24
B-700	Na^+	3.5	77.74±24.05	19.15±6.83	2.87±0.33	0.24±0.12
		10	80.29±25.03	17.63±6.67	1.52±0.19	0.56±0.18
	Ca^{2+}	3.5	80.34±25.03	16.88±6.39	2.49±0.26	0.29±0.11
		10	74.91±23.34	19.02±6.99	5.53±0.65	0.54±0.13